Author's accepted manuscript version	Merino D, Best SA, Asselin-Labat ML, Vaillant F, Pal B, Dickins RA, Anderson RL, Strasser A, Bouillet P, Lindeman GJ, Visvader JE. Pro-apoptotic Bim suppresses breast tumor cell metastasis and is a target gene of SNAI2. Oncogene. 2015 Jul 23;34(30):3926-34.
Final published version	doi: 10.1038/onc.2014.313 http://www.nature.com/articles/onc2014313
Copyright	© 2015 Macmillan Publishers Limited, part of Springer Nature. All Rights Reserved.
Terms of use	http://www.nature.com/reprints/index.html

Pro-apoptotic *Bim* suppresses breast tumor cell metastasis and is a target gene of SNAI2

Delphine Merino[1,2,6], Sarah A Best[1,2,6], Marie-Liesse Asselin-Labat[1,2], François Vaillant[1,2], Bhupinder Pal[1,2], Ross A Dickins[1,2], Robin L Anderson[3], Andreas Strasser[1,2], Philippe Bouillet[1,2], Geoffrey J Lindeman[1,4,5,6] and Jane E Visvader[1,2,6,*]

[1] The Walter and Eliza Hall Institute of Medical Research, Parkville, VIC 3052, Australia

[2] Department of Medical Biology, University of Melbourne, VIC 3010, Australia

[3] Peter MacCallum Cancer Centre, Melbourne, VIC 3002, Australia

[4] Department of Medical Oncology, Royal Melbourne Hospital, Parkville, VIC 3050, Australia

[5] Department of Medicine, University of Melbourne, VIC 3010, Australia

[6] These authors contributed equally to this study

[*] Correspondence: visvader@wehi.edu.au or lindeman@wehi.edu.au

Keywords: BIM, SNAI2, metastasis, breast cancer, disseminated tumor cells.

ABSTRACT

Evasion of cell death is fundamental to the development of cancer and its metastasis. The role of the BCL-2-mediated (intrinsic) apoptotic program in these processes remains poorly understood. Here we have investigated the relevance of the pro-apoptotic protein BIM to breast cancer progression using the MMTV-Polyoma middle-T (PyMT) transgenic model. BIM deficiency in PyMT females did not affect primary tumor growth, but substantially increased the survival of metastatic cells within the lung. These data reveal a role for BIM in the suppression of breast cancer metastasis. Intriguingly, we observed a striking correlation between the expression of BIM and the EMT transcription factor SNAI2 at the proliferative edge of the tumors. Overexpression and knockdown studies confirmed that these two genes were coordinately expressed, and ChIP analysis further revealed that *Bim* is a target of SNAI2. Taken together, our findings suggest that SNAI2-driven BIM–induced apoptosis may temper metastasis by governing the survival of disseminating breast tumor cells.

INTRODUCTION

Evasion of cell death is a major mechanism that contributes to tumor initiation and progression to a metastatic state. Metastasis is the culmination of a complex cascade that enables cancer cells to disseminate from the primary tumor site and proliferate at distant sites.[1] Cell survival is necessary at each of the steps in this cascade, including local invasion, entry and passage in the circulation, extravasation into secondary tissues, the formation of micrometastases and eventual colonization.[2] The vast majority of cancer cells that exit a primary tumor are destined to die, with most of this death occurring when circulating tumor cells in the blood arrive at distant organs. Tumor cells must then survive in the foreign microenvironment of the distant organ to form micrometastases. The role of the BCL-2 apoptotic pathway during the different stages of the metastatic cascade has yet to be elucidated.

Apoptosis is controlled by the BCL-2 protein family that encompasses one pro-survival and two pro-apoptotic subgroups. The pro-survival family members (e.g. BCL-2, BCL-XL, MCL-1) protect cells against apoptosis. The pro-apoptotic BCL-2 family members are divided into two sub-groups. The multi-BH (BCL-2 Homology) domain proteins BAX and BAK, are required for mitochondrial outer membrane permeabilization,[3] which leads to activation of the caspase cascade, cleavage of hundreds of cellular proteins and ultimately cell demolition. The BH3-only proteins include BIM, PUMA and BMF. BIM is a potent cell death initiator, in part due to its ability to bind all pro-survival BCL-2-like proteins with high affinity and its potential for direct activation of BAX and BAK.

Although BIM has been extensively studied in hematological malignancies,[4] relatively little is known about its role in solid tumors. Cell culture assays have identified BIM as a potential tumor suppressor, while *in vivo* studies have generated discordant data. In one report, loss of BIM accelerated tumor growth of transformed kidney cells[5] while another suggested that BIM behaved as a pro-survival protein,[6] in contrast to the well-established role of BIM as an essential initiator of apoptosis. Other reports have suggested that down-regulation of BIM is necessary for tumor progression. For example, comparison of BIM levels in early, primary and metastatic melanoma revealed a progressive decrease in BIM

expression,[7] with similar observations made for renal[8] and colon carcinoma cells.[9] Overall, these studies support the notion that BIM plays an important role in suppressing tumorigenesis.

In this study, we investigated the role of BIM in breast cancer progression using the *MMTV-PyMT* (denoted PyMT) transgenic mouse model, which recapitulates oncogenesis from preneoplasia to the advanced stages of breast cancer, including metastases to the lungs and lymph nodes.[10] Loss of BIM on the PyMT background was associated with a striking increase in metastasis due to increased survival of disseminated tumor cells within the lung. Moreover, we unraveled a molecular link between BIM and the epithelial to mesenchymal transition (EMT) transcription factor SNAI2, both of which were found to be upregulated at the tumor border. SNAI2 appears to be a direct regulator of *Bim* expression in breast epithelial cells, suggesting a novel function for this transcription factor at the proliferative edge of tumors, distinct from its role in the EMT. Thus, SNAI2 and BIM may act as suppressors of cancer cell exit from the primary tumor site and metastasis by promoting apoptosis.

RESULTS

Bim-deficiency does not impact on the growth of PyMT tumors

To examine the effect of BIM deletion on mammary tumorigenesis, we backcrossed *Bim* knockout mice (C57BL/6 background) onto a FVB/N background and then intercrossed these with PyMT transgenic mice. Western blot analysis confirmed the deletion of BIM from tumors of PyMT; $Bim^{-/-}$ mice and showed no change in the expression of other Bcl-2 family members in tumors of different genotypes (Figure 1A). Tumors developed in PyMT mice lacking one or two alleles of *Bim* with the same latency as in control PyMT mice (Figure 1B and 1C). Moreover, the tumors displayed similar histopathology based on immunostaining for lineage markers (Figure 1D).

Since *Bim* knockout mice on a C57BL/6 background are known to accumulate lymphoid and myeloid cells,[11] differences in the growth of primary PyMT tumors may be masked by hyperactivity of the host immune system. We therefore enumerated white blood cells

(WBC) in *Bim*-deficient mice on the FVB/N background. *Bim* deletion led to an increase in WBC numbers on this background (~2-fold), but this was less pronounced than that observed on the C57BL/6 background (~4-fold) (Supplementary Figure 1A). The overall increase in WBC numbers in PyMT; $Bim^{+/+}$ and PyMT; $Bim^{-/-}$ tumor-bearing mice may be due to the activation of an anti-tumor response. In the PyMT model, the recruitment of Gr-1^{+}CD11b^{+} myeloid cells to primary tumors has been implicated in metastasis development.[12] Since the number of myeloid cells is increased in *Bim*-deficient mice,[11, 13] we determined whether loss of BIM induced a greater accumulation of these cells in primary tumors. The numbers of Gr-1^{+}CD11b^{+} myeloid cells recruited to tumors developing in PyMT; $Bim^{+/+}$, PyMT; $Bim^{+/-}$ or PyMT; $Bim^{-/-}$ mice were found to be similar (Supplementary Figure 1B). Furthermore, transplantation of tumors of different genotypes into immunodeficient $Rag1^{-/-}$J mice showed that *Bim*-deficient tumors developed at the same rate as control PyMT tumors (Supplementary Figure 1C), thus indicating that the increase in leukocyte numbers accompanying loss of BIM does not appreciably alter the growth of PyMT tumors.

BIM and SNAI2 are highly expressed at the border of PyMT tumors

Although loss of BIM did not affect primary tumor growth, we unexpectedly found that BIM levels were notably higher at the tumor border. Concomitantly, expression of the EMT transcription factors SNAI2 and TWIST, and the proliferation marker KI67 were elevated (Figure 2A and 2B), whereas expression of the cell junctional protein β-CATENIN remained unchanged (Figure 2A and 2B). The 'proliferative edge effect' of increased SNAI2, TWIST and KI67, was observed in the PyMT and MMTV-Wnt1 mammary tumorigenesis models, but not in tumors from BALB/c-$p53^{+/-}$ or MMTV-Neu mice (Supplementary Figure 2A and 2B). Moreover, PyMT and Wnt1 tumors exhibited minimal levels of SNAI2 by Western blot analysis, compared to the pre-neoplastic state where high levels of SNAI2 protein were apparent (Supplementary Figure 2B). No change in SNAI2 levels was observed in the models that did not exhibit the 'proliferative edge effect'. Nevertheless, localized SNAI2-positive cells could be readily identified at the border of PyMT tumors (Supplementary Figure 2A). Since immunostaining for cleaved caspase 3 and TUNEL assay did not reveal an increase in cell death towards the

border of PyMT tumors (Supplementary Figure 2C), we surmise that cells may die upon exit from the tumor and be cleared rapidly. Interestingly, the vasculature was observed to be dense near the tumor border, as indicated by staining for CD31 (Supplementary Figure 2D).

Co-regulation of SNAI2 and BIM expression

We next investigated a potential relationship between SNAI2 and BIM expression as SNAI2 is a key regulator of mammary 'stemness' and the EMT.[14] Both SNAI2 and BIM are highly expressed in the virgin mammary gland, the tumor edge and micrometastases in the lung (Supplementary Figure 3A). Reduced BIM protein levels were observed in the human breast cancer cell line MDA-MB-231 following transfection with a human LMS-shSNAI2 construct (Supplementary Figure 3B). Moreover, knock-down of SNAI2 in sorted mouse MaSC/basal cells, which express high levels of SNAI2,[15] led to a marked reduction in BIM levels compared to cells transduced with a control virus (Figure 3A). Quantitative RT-PCR analysis of MaSC/basal cells in which SNAI2 was either suppressed (via LMS-shSNAI2) or overexpressed (via MIG-SNAI2) (Figure 3B) further showed a strong correlation between *Bim* and *Snai2* transcript levels. Interestingly, a 3-fold increase in dead or dying cells (double-positive for AnnexinV and PI) was observed in MIG-SNAI2 transduced MaSC/basal cells after a three-day culture period (Figure 3C), suggesting that SNAI2 can promote cell death via induction of BIM. To test this directly, we overexpressed SNAI2 in wild-type (WT), $Bim^{-/-}$ and $Bax^{-/-}Bak^{-/-}$ mouse embryonic fibroblasts (MEFs) (Figure 3D). As expected, SNAI2 over-expression killed a substantial proportion of WT MEFs, as measured by AnnexinV/PI staining. The reduced cell death evident in $Bim^{-/-}$ or $Bax^{-/-}Bak^{-/-}$ MEFs over-expressing SNAI2 suggests that cell death is due to BAX/BAK-mediated apoptosis, and that BIM is the main initiator of this process.

To investigate whether there might be a direct transcriptional relationship between SNAI2 and *Bim*, chromatin immuno-precipitation (ChIP) of SNAI2 on the *Bim* promoter was performed. Endogenous SNAI2 protein was found to bind to two regions upstream of the *Bim* transcriptional start site (TSS) (Figure 3E), also confirmed using cells transduced with a low copy number of a Flag-tagged version of SNAI2. In the context of human

breast cancer cells, ChIP was performed on MDA-MB-231-Luc cells for endogenous SNAI2 protein. This identified two regions upstream of the human *BIM* transcriptional start site that appear to be homologous to those mapped in the mouse *Bim* promoter (Supplementary Figure 3C). Collectively, our data suggest that *Bim* is a novel target gene of SNAI2 in both normal and neoplastic cells, and that SNAI2 may directly contribute to the upregulation of BIM at the border of PyMT tumors.

To determine whether *Bim* deficiency altered proliferation or EMT gene expression along the proliferative border, immunostaining for KI67, TWIST and SNAI2 was performed on tumors from PyMT; $Bim^{+/+}$ and PyMT; $Bim^{-/-}$ mice. A comparable extent of proliferation (Figure 4A) and enrichment for SNAI2 and TWIST expression (Figure 4B, Supplementary Figure 3D) was evident, regardless of the status of *Bim*. These findings are consistent with BIM acting downstream of SNAI2 and the EMT at the tumor border.

To determine whether these observations extended to human breast cancer, we performed immunostaining on 10 patient derived xenograft (PDX) models for KI67, SNAI2 and BIM. Interestingly, the 'proliferative edge effect' was only observed in metaplastic tumors (162T and 371T), and not in triple negative (T10T) or ER-positive tumors (23T) (Supplementary Figure 4). We speculate that SNAI2 and BIM expression at the tumor edge may play a role in tumor cell dissemination of specific human tumor subtypes such as in highly aggressive metaplastic breast tumors.

***Bim* deletion in PyMT tumors increases lung metastases**

The tumor border is presumed to play a critical role in dissemination of cells from the primary tumor site. To explore a potential role for BIM in metastasis, metastatic lesions in the lungs were evaluated by histological sectioning after primary PyMT tumors had reached ethical endpoint. The number of lung metastases was significantly increased (4-fold) in PyMT; $Bim^{-/-}$ mice compared to those observed in control PyMT; $Bim^{+/+}$ mice (Figure 5A and 5B), suggesting that *Bim* can suppress tumor metastasis in the absence of any effect on primary tumor growth (Figure 5C and Figure 1). It is noteworthy that loss of BIM did not alter the extent of tumor vascularization (Supplementary Figure 1D),

indicating that other factors contribute to the increased metastastic burden observed in *Bim*-deficient PyMT mice.

We next utilized the 'tail vein' metastasis assay to monitor dissemination of PyMT tumor cells to the lungs.[16] Mammary tumor cell suspensions from either PyMT; $Bim^{+/+}$ or PyMT; $Bim^{-/-}$ mice were injected into $Rag1^{-/-}$J recipient mice and lung tissue was analysed one month post-injection. Many more metastases were evident in the lungs of mice injected with PyMT; $Bim^{-/-}$ tumor cells compared to PyMT; $Bim^{+/+}$ cells, thus leading to significantly higher lung weights in *Bim*-deficient mice (Figure 6A, Supplementary Figure 5). These data indicate that *Bim*-deficient cells have markedly higher invasive capacity than control PyMT tumor cells. In the tail vein injection assay, most cells reach the lung vasculature within five minutes following injection, and then the majority of cells die within the next 24 hours.[17, 18] Therefore our data indicate that loss of BIM promotes the survival of metastatic cells during transit in the circulation and/or upon arrival of the tumor cells at the secondary organ.

To gain further insight into the rate of tumor cell attrition on extravasation, we turned to MDA-MB-231 cells carrying a luciferase gene cassette (MDA-MB-231-Luc), which enables *in vivo* imaging. Knock-down of BIM via stable shRNA expression (Supplementary Figure 6A) significantly enhanced tumor survival 48 hours post-injection in the tail vein metastasis assay compared to cells transduced with a control virus (Supplementary Figure 6B). However, no effect on the size of lung metastases was observed when the cells were transplanted into the mammary fat pad (data not shown). Following tail vein injection, the luciferase signal could be readily detected in the lungs after injection of 1×10^6 cells. This signal in the lungs was found to decrease over the next 24 hours in control cells, before increasing again as metastatic growth ensued (Supplementary Figure 6B). The observation that some control cells could survive in the lungs suggests that the threshold of BIM in these cells was not sufficient to induce apoptosis. Collectively, BIM appears to play an important role in the induction of apoptosis of tumor cells following intravasation into the bloodstream.

Bim deletion in PyMT tumors increases the survival of disseminated cells

To evaluate the survival of *Bim*-deficient tumor cells once they had extravasated, PyMT; $Bim^{+/+}$ and PyMT; $Bim^{-/-}$ breast tumor cells were injected directly into the lung by intratracheal injection. Mice that received *Bim*-deficient cells tended to be the first to exhibit symptoms of respiratory distress. One month post-injection, the majority of mice injected with PyMT; $Bim^{-/-}$ tumor cells developed large metastases within their lungs while those injected with PyMT; $Bim^{+/+}$ tumor cells only had small lesions (Figure 6B). Consequently, the weight of the lungs was substantially higher in the group of mice injected with cells from PyMT; $Bim^{-/-}$ mice. BIM is therefore a critical regulator of apoptosis in tumor cells capable of seeding lung metastases.

DISCUSSION

There is accumulating evidence that tumor cells can disseminate at early stages of neoplasia, despite the metastatic process originally being considered a late event in the progression of breast cancer.[19] A large number of potentially metastatic cells reach the circulation, but only a minute proportion of them are capable of seeding and growing in distant organs. The elimination of cancer cells in a new environment has been termed 'metastasis inefficiency'.[20] Apoptosis of tumor cells is thought to be central to 'metastasis inefficiency', and over-expression of either BCL-2 or BCL-XL has been shown to increase tumor cell colonization of the lungs following tail vein injection.[18, 21-24] Here we report that BIM-mediated apoptosis contributes to 'metastasis inefficiency' by limiting the survival of mammary tumor cells at secondary sites of metastasis.

In the PyMT mouse model of mammary tumorigenesis, loss of BIM led to an increase in the number of lung metastases. Using assays that specifically allow assessment of tumor cell entry into the lungs and subsequent colonization (injection of cells directly into the blood or trachea), ablation of *Bim* was found to significantly enhance the survival of disseminated cells within the lung environment. The processes that have been implicated in facilitating the survival of disseminated cancer cells primarily reflect attenuation of death signals from the reactive stroma. For example, brain metastases in breast cancer appear to express serpins to prevent the mobilization of FasL by plasmin from reactive

astrocytes.[25] Amplification of PI3K-AKT pathway activity in disseminated tumor cells plays a prominent role in their survival upon entry into the foreign environment of the distant organ. In lung metastases, macrophage-mediated engagement of VCAM1 triggers AKT activation in tumor cells to protect them against TRAIL-induced apoptosis,[26] while in the bone marrow, SRC amplifies the PI3K-AKT response of breast cancer cells to counteract apoptotic signals from TRAIL and CXCL12.[27] TrkB can function as an inhibitor of anoikis in detached tumor cells, in part through activation of AKT,[28] which may result in inhibition of BIM expression.[29] More recently, the acute activation of miR-31 in established lung metastases was shown to induce regression by decreasing AKT signaling and increasing BIM levels.[30] This finding supports our data and highlights the importance of BIM in the survival of disseminated cells in the lung microenvironment.

BIM deletion did not impact on primary tumor growth or latency in the PyMT model. Consistent with these findings, down-regulation of BIM in MDA-MB-231-Luc cells did not affect primary tumor growth (data not shown). In the PyMT model, mice were sacrificed due to their primary tumors reaching ethical endpoint, thus precluding analysis of the effect of metastatic burden on overall survival of PyMT; $Bim^{+/+}$ versus PyMT; $Bim^{-/-}$mice. Nevertheless, tumors appeared with the same latency for both genotypes, and reached ethical endpoint at similar time. These data differ from a previous report showing that Bim suppresses tumorigenesis of transformed mouse kidney cells upon subcutaneous transplantation,[5] and may reflect differences in the oncogenic lesions that drive tumorigenesis or the mode of transplantation of tumor cells. Conversely, other studies showed that BCL-2 and BCL-XL overexpression increased metastasis without affecting the primary tumor growth[18, 31] consistent with the data presented here. The observation that loss of BIM enhances metastasis without affecting primary tumor growth might be explained by differences in the expression of BIM between primary tumor and metastatic cells. Loss of extracellular matrix contact is known to induce BIM during anoikis through a decrease in 14-3-3zeta and inhibition of ERK and PI3K signaling.[32-36] Even though post-translational regulation of BIM by ERK phosphorylation may be dispensable in the normal hemopoietic system,[37] it could be important in a neoplastic context. The levels of pro-apoptotic BAD and BMF, as well as those of the pro-survival molecules MCL-1 and

BCL-XL, also have been implicated in inducing anoikis.[33, 35, 38-40]

A novel transcriptional link between the transcription factor SNAI2 and pro-apoptotic BIM was revealed in both normal mouse mammary epithelial cells and breast cancer cells. Moreover, higher levels of both SNAI2 and BIM were evident at the proliferative edge of the tumor. Interestingly, an association was noted between SNAI2 and BIM expression at the border of highly aggressive metaplastic breast cancers from patients. SNAI2 is a key regulator of the EMT,[41] and its expression is linked to the progression of solid tumors and the risk of metastatic relapse.[42] In *BRCA1*-associated tumors, the higher levels of SNAI2 protein present have suggested that *Snai2* contributes to aberrant differentiation of luminal cells towards the basal lineage.[43] In other contexts, SNAI2 has been implicated in the radioresistance of hematopoietic cells,[44] in which SNAI2 may serve an anti-apoptotic function. SNAI2 may protect cells from apoptosis by repressing P53-mediated transcription of PUMA, a BH3-only protein that is essential for DNA damage-induced and P53-mediated apoptosis.[45] More recently, SNAI2 regulation of PUMA was shown to be stimulated by N-cadherin in breast tumors.[46] Therefore during breast tumorigenesis, SNAI2 may have dual functions in promoting a mesenchymal phenotype via an EMT as well as regulating the expression of BCL-2 family members, dependent on external stimuli. The lack of discernible apoptosis at the tumor edge suggests that SNAI2 and BIM-expressing cells may be protected by the expression of pro-survival proteins. Pertinently, high levels of SNAI2 could trigger BIM-mediated apoptosis in normal basal epithelial cells as well as in MEFs. It is tempting to speculate that cells at the mammary tumor border are primed for cell death, rendering them more sensitive to environmental stimuli when they reach the circulation, as recently described for metastatic colon cancer cell lines.[47]

Our findings that BIM influences the survival of tumor cells following extravasation into the lungs suggest that the loss of BIM may be responsible for early dissemination of tumor cells and their colonization of distant tissues. It will be of interest to determine whether mutations or epigenetic silencing of *BIM* during metastasis correlate with poor outcome in patients with breast cancer (and other malignancies). Inhibition of BIM-

induced cell death in metastasis is likely to be one mechanism to facilitate tumor cell spreading. Other mechanisms may include the upregulation of pro-survival proteins such as BCL-2, high levels of which have been observed in metastatic breast cancer.[48-50] The identification of further regulators that control the survival of metastatic cells has the potential to yield new therapeutic strategies to target tumor dissemination.

MATERIALS AND METHODS

Mice and tumor monitoring

MMTV-PyMT [FVB/NJ] and BIM knockout [C57BL/6] mice have been described.[10] The PyMT;Bim strain was generated by crossing $Bim^{-/-}$ 266Del [C57BL/6] mice[11] onto the FVB/N background for 8 generations before crossing with MMTV-PyMT transgenic mice. In some cases (where indicated), tumor cells were obtained from F2 (second generation) mice that resulted from crosses between MMTV-PyMT and $Bim^{-/-}$ 266Del mice. For transplantation studies, $Rag1^{-/-}$J mice or NOD/SCID/IL2$\gamma^{-/-}$ mice were used. Mice were palpated three times a week for tumor detection and measurement. The date when tumors were first detected was recorded for the generation of tumor-free survival curves. Tumors were collected at the ethical endpoint of 600 mm^3. Blood count analysis was performed on an Advia 2120 blood analysis machine (Siemens, Germany). All animal experiments were conducted with the approval and according to the guidelines of the WEHI Animal Ethics Committee.

Cell lines

The MDA-MB-231-Luc cell line (Caliper Life Sciences, USA) was maintained in RPMI-1640 plus GlutaMAX-1 (Gibco, USA), supplemented with 10 % fetal calf serum (FCS). BIM down-regulation was performed using the pSuper shRNA expression construct.[51] For SNAI2 knockdown, hairpins were cloned into the LMS vector: mouse 5'-TGCTGTTGACAGTGAGCGCCCAGAATGTCGCTTCTGCATATAGTGAAGCCAC AGATGTATATGCAGAAGCGACATTCTGGATGCCTACTGCCTCGGA-3' and human 5'-TGCTGTTGACAGTGAGCGTAGACAGACAATCATATTAATCTAGTGA-AGCCACAGATGTAGATTAATATGATTGTCTGTCTATGCCTACTGCCTCGGA-3' and with the renilla luciferase (non-mammalian target) control 5'-

TCGAGAAGGTATATTGCTGTTGACAGTGAGCGCAGGAATTATAATGCTTATCT ATAGTGAAGCCACAGATGTATAGATAAGCATTATAATTCCTATGCCTACTGCC TCGG-3'. Primary MaSC/basal cells were isolated from the inguinal and thoracic mammary glands of 8 week-old FVB/N mouse. Cell culture and retroviral infections were performed on feeder layers of irradiated fibroblasts prior to sorting for transduced cells, as previously described.[52]

Cell death assays were performed by staining with APC-conjugated AnnexinV (BD Biosciences, USA) at RT for 30 min in 2 mM $CaCl_2$/PBS solution and resuspended in Propidium Iodide (PI; 1 μg/mL). Flow cytometric analysis was performed in an LSR II Analyzer (BD Biosciences) and AnnexinV$^-$ PI$^-$ cells were considered to be alive.

Mouse cell lines were transduced with retrovirus produced in Phoenix cells, while human cell lines were transfected using Lipofectamine LTX Reagent (Invitrogen, USA) according to manufacturer's protocols.

Preparation of single cell suspensions and cell transplantation

Single cell suspensions from *MMTV-PyMT* tumors were prepared by digestion in 150 U/ml collagenase (Sigma, USA) and 50 U/ml hyaluronidase (Sigma) for 1 - 2 h at 37^o C. The resulting organoid suspension was sequentially digested with 0.25 % trypsin/1 mM EGTA and 5 mg/mL dispase (Roche Diagnostics, Switzerland) for 1 min at 37 °C. A single cell suspension was obtained by filtration (40 μm) and red blood cells were removed by incubation in red blood cell lysis buffer. Cell suspension were frozen in 50 % serum, 44 % culture medium and 6 % DMSO.

For transplantation assays, 500,000 tumor cells were resuspended in 10 μL of transplantation buffer (50 % FCS, 0.04 % trypan blue in PBS and Matrigel (BD) at a ratio of 3:1), and injected into the cleared mammary fat pads of 3 - 4 week-old Rag1$^{-/-}$J (for PyMT; Bim$^{+/+}$ and PyMT; Bim$^{-/-}$ tumor cells). For intravenous (i.v.) injections into the tail vein, 500,000 PyMT tumor cells were injected into Rag1$^{-/-}$J or 1 x 10^6 MDA-MB-213-luc cells were injected into NOD-SCID-IL2R$\gamma_c^{-/-}$. For intratracheal injections, 1 x

10^6 cells were resuspended in 50 % Matrigel and 50 % PBS, before injection by a canula into the trachea, as previously described.[53] In each case, mice were sacrificed when the tumor volume reached 600 mm^3 or their health had deteriorated.

Patient derived xenograft models

Human breast tumors were obtained from consenting patients through the Royal Melbourne Hospital Tissue Bank and the Victorian Cancer Biobank with relevant institutional review board approval. Human Ethics approval was obtained from the Walter and Eliza Hall Institute (WEHI) Human Research Ethics Committee. Human breast tumor fragments were inserted into the inguinal mammary fat pads of 4-week-old NOD-SCID-IL2R$\gamma_c^{-/-}$ female mice and passaged as previously described.[54] Passage 2 tumors were collected at ethical endpoint for immunohistochemistry.

Immunohistochemistry

Human xenografted tumors were collected and fixed in formalin before embedding in paraffin. Sections were subjected to antigen retrieval and then incubated with antibodies against either BIM (Cell Signaling), KI67 (Dakocytomation), KERATIN 8 (Promega), P63 (Abcam), TWIST1 (Novus Biologicals), SNAI2 (Cell Signaling), β-CATENIN (BD Biosciences) or CD31 (BD Pharmingen) followed by incubation with biotinylated anti-IgG secondary antibodies (Vector Labs, USA). Signal detection was performed using ABC Elite (Vector Labs) and 3,3'-diaminobenzidine (DAB) (Dako, Denmark). For immunofluorescence, primary antibodies (CD31, BD Pharmingen; KI67, Cell Signaling) were incubated at 4°C overnight and secondary antibodies (Life Technologies) and DAPI (Sigma) were incubated for 30 minutes at RT, before being mounted with Fluoromount-G (Southern Biotech) for fluorescence microscopy.

For histological examination of the metastases, organs were fixed in 4 % paraformaldehyde, embedded in paraffin, sectioned (1.5 μm) and stained with haematoxylin and eosin. For quantification of KI67 positive cells, immunohistochemical images were separated into two color filters (one representing the haematoxylin/nuclei stain, the other the DAB stain), using a Color Deconvolution module. The individual

channel images were then inverted and the number of positive and negative cells was counted using the Multi Wavelength Cell Scoring application module from MetaMorph™ v7.7.10.0 (Molecular Devices, USA). For TWIST, SNAI2, BIM, KI67 and β-CATENIN border analysis, quantification was performed using the Colour Deconvolution module in Fiji software (Softonic Inc, Spain) and analysis by the MetaMorph™ v7.7.10.0 line scan.

Terminal deoxynucleotidyl transferase-mediated dUTP nick end labeling (TUNEL)

In situ cell death detection kit (Roche) was used to perform the TUNEL assay, according to the manufacturer's protocol. Slides were imaged on Zeiss Axio Scan.Z1 and analyzed using Zen software (Zeiss).

***In vivo* imaging**

Mice and organs were imaged at different time points using the Xenogen IVIS Spectrum live imager (Caliper Life Sciences). Mice were injected intraperitoneally with Luciferin (Caliper Life Sciences, 15 mg/ml) 10 min prior to imaging. For lung imaging, mice were injected with Luciferin before euthanasia and imaging of the organs.

Immunoblot analysis

Tumors were homogenized in lysis buffer (20 mM Tris.HCl, 135 mM NaCl, 1.5 mM MgCl2, 1 mM EGTA, 1 % Triton X-100 and 10 % glycerol). Protein lysates were analyzed by western blot analysis on 12 % SDS-polyacrylamide gels (Invitrogen), and transferred onto PVDF membranes (Millipore, USA). Membranes were probed with anti-BIM (C34C5, Cell Signaling Technologies), anti-BCL-2 (BCL-2-100, WEHI Monoclonal Antibody Facility), anti-BCL-XL (54H6, Cell Signaling Technologies), anti-MCL-1 (14C11-20, WEHI Monoclonal Antibody Facility), anti-BAX (554106, BD Biosciences), anti-SNAI2 (C19G7, Cell Signaling Technologies) or anti-ACTIN (Sigma).

Quantitative RT-PCR

RNA was extracted from cell pellets of MaSC/basal cells using the RNeasy RNA extraction kit (Qiagen) and cDNA generated using the First Strand kit (Life

Technologies) according to the manufacturer's instructions. qRT-PCR was performed using SyberGreen (Bioline, UK) on the Corbett RotorGene qPCR machine and software (Life Technologies, USA). Relative mRNA was calculated compared to *Gapdh* internal control. Primers used were *Gapdh* 5'-TGACATCAAGAAGGTGGTGAAGC-3' R 5'-AAGGTGGAAGAGTGGGAGTTGCTG-3'; *Snai2* F 5'-CCTTTCTCTTGCCCTCACTG-3' R 5'-ACAGCAGCCAGACTCCTCAT-3'; *Bim* F 5'-GAGTTGTGACAAGTCAACACAAACC-3' R 5'-GAAGATAAAGCGTAACAGTTGTAAGATAAC-3'.

Chromatin immuno-precipitation (ChIP) analysis

ChIP was performed on 1 x 10^6 CommaDβGeo cells or MDA-MB-231 cells as described previously,[55] with shearing optimized for approximately 500 bp fragments, using anti-IgG (Cell Signaling), anti-SNAI2 (Cell Signaling) and anti-FLAG (Sigma). Primers used for CommaDβGeo PCR were: -300 bp F 5'-AAGGGCGGAGGGACGCC-3' R 5'-GCGACAGGTAGTGGGGAG-3'; -1200 bp F 5'-CCGTGACGTTAGATCCGC-3' R 5'-CTTTGTGATTCCAACAG-3' and for MDA-MB-231 PCR: -300 F 5'-GATGACGCTAAATCAGTTG-3' R 5'-GTGATGGATCAGTATACAG-3'; -800 bp F 5'-GCATTGCAGTTGTTCAGG-3' R 5'-CGTATGGGTGGGGCGTGG-3'; TSS F 5'-CTTACTTGTGTTTTGCAC-3' R 5'-CTAGTTGAAAGTTTTATT-3'.

Statistical analyses

Statistical analyses were performed in Prism (GraphPad Software, USA). Kaplan-Meier (log-rank test) was used for testing the significance of animal survival related to the ethical end point for tumor size. Unpaired t tests were used to test the significance of column means between treatment and control. Significance is indicated by the following convention: *p<0.05; **p<0.01; ***p<0.001.

CONFLICT OF INTEREST

The authors declare no conflict of interest.

ACKNOWLEDGEMENTS

We are grateful to K Rogers, L Whitehead, C Nowell for help with imaging, K Birchall, L Reid, and G Siciliano for animal husbandry, B Helbert and C Young for mouse genotyping, K Breslin, M Robati and K Liu for technical assistance. We thank D Metcalf and JM Adams for useful discussion and advice, LA O'Reilly for antibodies and D Huang for knockout MEF cell lines. This work was supported by the National Health and Medical Research Council, Australia (NHMRC, 461221 and 1016701); NHMRC IRIISS; the Victorian State Government through Victorian Cancer Agency funding of the Victorian Breast Cancer Research Consortium and Operational Infrastructure Support; the Australian Cancer Research Foundation; and The National Breast Cancer Foundation. DM was supported by a NBCF Early Career Fellowship, RLA by a senior NBCF Fellowship, and SB by a NHMRC Postgraduate Scholarship #1017256. JEV and GJL were supported by an NHMRC Australia Fellowship and Research Fellowship (637307), respectively.

REFERENCES

1 Vanharanta S, Massague J (2013). Origins of metastatic traits. *Cancer Cell* **24:** 410-421.

2 Mehlen P, Puisieux A (2006). Metastasis: a question of life or death. *Nat Rev Cancer* **6:** 449-458.

3 Chipuk JE, Bouchier-Hayes L, Green DR (2006). Mitochondrial outer membrane permeabilization during apoptosis: the innocent bystander scenario. *Cell Death Differ* **13:** 1396-1402.

4 Pinon JD, Labi V, Egle A, Villunger A (2008). Bim and Bmf in tissue homeostasis and malignant disease. *Oncogene* **27 Suppl 1:** S41-52.

5 Tan TT, Degenhardt K, Nelson DA, Beaudoin B, Nieves-Neira W, Bouillet P *et al* (2005). Key roles of BIM-driven apoptosis in epithelial tumors and rational chemotherapy. *Cancer Cell* **7:** 227-238.

6 Gogada R, Yadav N, Liu J, Tang S, Zhang D, Schneider A *et al* (2013). Bim, a proapoptotic protein, up-regulated via transcription factor E2F1-dependent

mechanism, functions as a prosurvival molecule in cancer. *J Biol Chem* **288:** 368-381.

7 Dai DL, Wang Y, Liu M, Martinka M, Li G (2008). Bim Expression Is Reduced in Human Cutaneous Melanomas. *J Invest Dermatol* **128:** 403-407.

8 Zantl N, Weirich G, Zall H, Seiffert BM, Fischer SF, Kirschnek S *et al* (2007). Frequent loss of expression of the pro-apoptotic protein Bim in renal cell carcinoma: evidence for contribution to apoptosis resistance. *Oncogene* **26:** 7038-7048.

9 Sinicrope FA, Rego RL, Okumura K, Foster NR, O'Connell MJ, Sargent DJ *et al* (2008). Prognostic impact of bim, puma, and noxa expression in human colon carcinomas. *Clin Cancer Res* **14:** 5810-5818.

10 Guy CT, Cardiff RD, Muller WJ (1992). Induction of mammary tumors by expression of polyomavirus middle T oncogene: a transgenic mouse model for metastatic disease. *Mol Cell Biol* **12:** 954-961.

11 Bouillet P, Metcalf D, Huang DC, Tarlinton DM, Kay TW, Kontgen F *et al* (1999). Proapoptotic Bcl-2 relative Bim required for certain apoptotic responses, leukocyte homeostasis, and to preclude autoimmunity. *Science* **286:** 1735-1738.

12 Yang L, Huang J, Ren X, Gorska AE, Chytil A, Aakre M *et al* (2008). Abrogation of TGF beta signaling in mammary carcinomas recruits Gr-1+CD11b+ myeloid cells that promote metastasis. *Cancer Cell* **13:** 23-35.

13 Bouillet P, Purton JF, Godfrey DI, Zhang L-C, Coultas L, Puthalakath H *et al* (2002). BH3-only Bcl-2 family member Bim is required for apoptosis of autoreactive thymocytes. *Nature* **415:** 922-926.

14 Guo W, Keckesova Z, Donaher JL, Shibue T, Tischler V, Reinhardt F *et al* (2012). Slug and Sox9 cooperatively determine the mammary stem cell state. *Cell* **148:** 1015-1028.

15 Lim E, Wu D, Pal B, Bouras T, Asselin-Labat ML, Vaillant F *et al* (2010). Transcriptome analyses of mouse and human mammary cell subpopulations reveals multiple conserved genes and pathways. *Breast Cancer Res* **12:** R21.

16 Smith MC, Luker KE, Garbow JR, Prior JL, Jackson E, Piwnica-Worms D *et al* (2004). CXCR4 regulates growth of both primary and metastatic breast cancer. *Cancer Res* **64:** 8604-8612.

17 Qian B, Deng Y, Im JH, Muschel RJ, Zou Y, Li J *et al* (2009). A distinct macrophage population mediates metastatic breast cancer cell extravasation, establishment and growth. *PLoS One* **4:** e6562.

18 Wong CW, Lee A, Shientag L, Yu J, Dong Y, Kao G *et al* (2001). Apoptosis: an early event in metastatic inefficiency. *Cancer Res* **61:** 333-338.

19 Husemann Y, Geigl JB, Schubert F, Musiani P, Meyer M, Burghart E *et al* (2008). Systemic spread is an early step in breast cancer. *Cancer Cell* **13:** 58-68.

20 Chambers AF, Naumov GN, Vantyghem SA, Tuck AB (2000). Molecular biology of breast cancer metastasis. Clinical implications of experimental studies on metastatic inefficiency. *Breast Cancer Res* **2:** 400-407.

21 del Bufalo D, Biroccio A, Leonetti C, Zupi G (1997). Bcl-2 overexpression enhances the metastatic potential of a human breast cancer line. *FASEB Journal* **11:** 947-953.

22 Fernandez Y, Espana L, Manas S, Fabra A, Sierra A (2000). Bcl-xL promotes metastasis of breast cancer cells by induction of cytokines resistance. *Cell Death Differ* **7:** 350-359.

23 Takaoka A, Adachi M, Okuda H, Sato S, Yawata A, Hinoda Y *et al* (1997). Anti-cell death activity promotes pulmonary metastasis of melanoma cells. *Oncogene* **14:** 2971-2977.

24 Townson JL, Naumov GN, Chambers AF (2003). The role of apoptosis in tumor progression and metastasis. *Curr Mol Med* **3:** 631-642.

25 Valiente M, Obenauf AC, Jin X, Chen Q, Zhang XH, Lee DJ *et al* (2014). Serpins promote cancer cell survival and vascular co-option in brain metastasis. *Cell* **156:** 1002-1016.

26 Chen Q, Zhang XH, Massague J (2011). Macrophage binding to receptor VCAM-1 transmits survival signals in breast cancer cells that invade the lungs. *Cancer Cell* **20:** 538-549.

27 Zhang XH, Wang Q, Gerald W, Hudis CA, Norton L, Smid M *et al* (2009). Latent bone metastasis in breast cancer tied to Src-dependent survival signals. *Cancer Cell* **16:** 67-78.

28 Douma S, Van Laar T, Zevenhoven J, Meuwissen R, Van Garderen E, Peeper DS (2004). Suppression of anoikis and induction of metastasis by the neurotrophic receptor TrkB. *Nature* **430:** 1034-1039.

29 McCubrey JA, Steelman LS, Chappell WH, Abrams SL, Wong EW, Chang F *et al* (2007). Roles of the Raf/MEK/ERK pathway in cell growth, malignant transformation and drug resistance. *Biochim Biophys Acta* **1773:** 1263-1284.

30 Valastyan S, Chang A, Benaich N, Reinhardt F, Weinberg RA (2011). Activation of miR-31 function in already-established metastases elicits metastatic regression. *Genes Dev* **25:** 646-659.

31 Martin SS, Ridgeway AG, Pinkas J, Lu Y, Reginato MJ, Koh EY *et al* (2004). A cytoskeleton-based functional genetic screen identifies Bcl-xL as an enhancer of metastasis, but not primary tumor growth. *Oncogene* **23:** 4641-4645.

32 Fukazawa H, Noguchi K, Masumi A, Murakami Y, Uehara Y (2004). BimEL is an important determinant for induction of anoikis sensitivity by mitogen-activated protein/extracellular signal-regulated kinase kinase inhibitors. *Mol Cancer Ther* **3:** 1281-1288.

33 Li Z, Zhao J, Du Y, Park HR, Sun SY, Bernal-Mizrachi L *et al* (2008). Down-regulation of 14-3-3zeta suppresses anchorage-independent growth of lung cancer cells through anoikis activation. *Proc Natl Acad Sci USA* **105:** 162-167.

34 Qi XJ, Wildey GM, Howe PH (2006). Evidence that Ser87 of BimEL is phosphorylated by Akt and regulates BimEL apoptotic function. *J Biol Chem* **281:** 813-823.

35 Reginato MJ, Mills KR, Paulus JK, Lynch DK, Sgroi DC, Debnath J *et al* (2003). Integrins and EGFR coordinately regulate the pro-apoptotic protein Bim to prevent anoikis. *Nat Cell Biol* **5:** 733-740.

36 Uehara N, Matsuoka Y, Tsubura A (2008). Mesothelin promotes anchorage-independent growth and prevents anoikis via extracellular signal-regulated kinase signaling pathway in human breast cancer cells. *Mol Cancer Res* **6:** 186-193.

37 Clybouw C, Merino D, Nebl T, Masson F, Robati M, O'Reilly L *et al* (2012). Alternative splicing of Bim and Erk-mediated Bim(EL) phosphorylation are dispensable for hematopoietic homeostasis in vivo. *Cell Death Differ*.

38 Boisvert-Adamo K, Longmate W, Abel EV, Aplin AE (2009). Mcl-1 is required for melanoma cell resistance to anoikis. *Mol Cancer Res* **7:** 549-556.

39 Puthalakath H, Villunger A, O'Reilly LA, Beaumont JG, Coultas L, Cheney RE *et al* (2001). Bmf: a pro-apoptotic BH3-only protein regulated by interaction with the myosin V actin motor complex, activated by anoikis. *Science* **293:** 1829-1832.

40 Sheridan C, Brumatti G, Martin SJ (2008). Oncogenic B-RafV600E inhibits apoptosis and promotes ERK-dependent inactivation of Bad and Bim. *J Biol Chem* **283:** 22128-22135.

41 Thiery JP, Acloque H, Huang RY, Nieto MA (2009). Epithelial-mesenchymal transitions in development and disease. *Cell* **139:** 871-890.

42 De Craene B, Berx G (2013). Regulatory networks defining EMT during cancer initiation and progression. *Nat Rev Cancer* **13:** 97-110.

43 Proia TA, Keller PJ, Gupta PB, Klebba I, Jones AD, Sedic M *et al* (2011). Genetic predisposition directs breast cancer phenotype by dictating progenitor cell fate. *Cell Stem Cell* **8:** 149-163.

44 Wu WS, Heinrichs S, Xu D, Garrison SP, Zambetti GP, Adams JM *et al* (2005). Slug Antagonizes p53-Mediated Apoptosis of Hematopoietic Progenitors by Repressing puma. *Cell* **123:** 641-653.

45 Villunger A, Michalak EM, Coultas L, Müllauer F, Böck G, Ausserlechner MJ *et al* (2003). p53- and drug-induced apoptotic responses mediated by BH3-only proteins Puma and Noxa. *Science* **302:** 1036-1038.

46 Kim S, Yao J, Suyama K, Qian X, Qian BZ, Bandyopadhyay S *et al* (2014). Slug Promotes Survival during Metastasis through Suppression of Puma-Mediated Apoptosis. *Cancer Res* **74:** 3695-3706.

47 Maamer-Azzabi A, Ndozangue-Touriguine O, Breard J (2013). Metastatic SW620 colon cancer cells are primed for death when detached and can be sensitized to anoikis by the BH3-mimetic ABT-737. *Cell Death Dis* **4:** e801.

48 Gasparini G, Barbareschi M, Doglioni C, Palma PD, Mauri FA, Boracchi P *et al* (1995). Expression of bcl-2 protein predicts efficacy of adjuvant treatments in operable node-positive breast cancer. *Clin Cancer Res* **1:** 189-198.

49 Leek RD, Kaklamanis L, Pezzella F, Gatter KC, Harris AL (1994). Bcl-2 in normal human breast and carcinoma, association with oestrogen receptor-positive, epidermal growth factor receptor-negative tumours and *in situ* cancer. *British Journal of Cancer* **69:** 135-139.

50 Silvestrini R, Veneroni S, Daidone MG, Benini E, Boracchi P, Mezzetti M *et al* (1994). The Bcl-2 protein: a prognostic indicator strongly related to p53 protein in lymph node-negative breast cancer patients. *J Natl Cancer Inst* **86:** 499-504.

51 Bouillet P, Robati M, Bath M, Strasser A (2005). Polycystic kidney disease prevented by transgenic RNA interference. *Cell Death Differ* **12:** 831-833.

52 Bouras T, Pal B, Vaillant F, Harburg G, Asselin-Labat ML, Oakes SR *et al* (2008). Notch signaling regulates mammary stem cell function and luminal cell-fate commitment. *Cell Stem Cell* **3:** 429-441.

53 Buckle T, van Leeuwen FW (2010). Validation of intratracheal instillation of lung tumour cells in mice using single photon emission computed tomography/computed tomography imaging. *Lab Anim* **44:** 40-45.

54 Oakes SR, Vaillant F, Lim E, Lee L, Breslin K, Feleppa F *et al* (2012). Sensitization of BCL-2-expressing breast tumors to chemotherapy by the BH3 mimetic ABT-737. *Proc Natl Acad Sci USA* **109:** 2766-2771.

55 Voss AK, Dixon MP, McLennan T, Kueh AJ, Thomas T (2012). Chromatin immunoprecipitation of mouse embryos. *Methods Mol Biol* **809:** 335-352.

Figure legends

Figure 1: BIM loss does not affect tumor formation in PyMT transgenic mice. (A) Expression of BIM, BCL-XL, BCL-2, MCL-1 and BAX in tumors from PyMT; $Bim^{+/+}$, PyMT; $Bim^{+/-}$ and PyMT; $Bim^{-/-}$ mice (n = 3 independent tumors). TUBULIN was used as the loading control. (B) Tumor latency in PyMT; $Bim^{+/+}$ (n = 16), PyMT; $Bim^{+/-}$ (n = 15) and PyMT; $Bim^{-/-}$ (n = 11) mice. $Bim^{-/-}$ mice (n = 3) did not develop mammary tumors. (C) Survival of PyMT; $Bim^{+/+}$ (n = 13), PyMT; $Bim^{+/-}$ (n = 11) and PyMT; $Bim^{-/-}$(n = 12) mice at the ethical endpoint. For all genotypes, mice were euthanized when the primary tumors reached 600 mm^3. (D) Immunostaining of PyMT; $Bim^{+/+}$ and PyMT; $Bim^{-/-}$ tumors for BIM, KERATIN 8 and P63 expression. H&E, hematoxylin and eosin stain. Scale bar, 40 μm.

Figure 2: BIM is upregulated at the border of PyMT tumors. (A) Immunostaining of tumors from PyMT; $Bim^{+/+}$ mice for KI67, TWIST, SNAI2 and BIM. Staining for β-CATENIN was included as a control as it exhibited uniform expression from the center to the border of tumors. Scale bar, 10 μm. (B) Statistical analysis of Metamorph linescan data from immunostained tumors from PyMT; $Bim^{+/+}$ mice with representative images shown in (A). Immunostained images were deconvoluted, and 16-color fluorescence used to measure the intensity of staining at the border of tumors relative to intensity at the centre. β-CATENIN immunostaining provided a control (n = 3-4 independent experiments). Data represent the mean ± SEM.

Figure 3: SNAI2 binds to the *Bim* promoter. (A) Western blot analysis of SNAI2 and BIM expression levels in MaSC-enriched/basal cells expressing either LMS-shLUC (renilla luciferase) or LMS-shSNAI2. ACTIN was used as a loading control. (B) Quantitative RT-PCR analysis of *Snai2* (left panel) and *Bim* (right panel) transcript levels in the MaSC/basal population expressing LMS-shLUC (control), LMS-shSNAI2 (construct), MIG-empty (control) or MIG-SNAI2 (construct) relative to *Gapdh* levels. Analysis is represented as fold change compared to the control in each group. Data represent the mean ± SEM for 3 independent experiments. (C) Cell death assay in

MaSC/basal cells expressing either MIG-empty or MIG-SNAI2. The percentage of AnnexinV^{+}PI^{+} cells was analysed by flow cytometry. Data represent the mean ± SEM for 5 independent transductions. (D) Cell death assay in mouse embryonic fibroblasts (MEFs). Wild type (WT), Bim$^{-/-}$ and Bax$^{-/-}$Bak$^{-/-}$ expressing either MIG-empty or MIG-SNAI2 were analyzed by flow cytometry for AnnexinV^{+}PI^{+} cells. Data represent the mean ± SEM for 3 independent experiments. (E) Chromatin immuno-precipitation (ChIP) of SNAI2 protein on different regions of the upstream regulatory region of *Bim* in mouse CommaDβgeo cells. Precipitation using anti-IgG was used as a control. CommaDβgeo cells expressing a low copy number of the Flag-tagged SNAI2 construct (MIG-SNAI2) were subjected to immunoprecipitation using anti-FLAG antibody, and parental CommaDβgeo cells were analysed using anti-SNAI2 antibody to detect endogenous SNAI2 protein binding (n = 2 independent experiments).

Figure 4: *Bim* loss does not affect proliferation and the expression of EMT markers in PyMT tumors. (A) KI67 immunostaining of tumors from PyMT Bim$^{+/+}$ and PyMT Bim$^{-/-}$ mice. Left panel, quantitation of KI67 positive cells per field. Data represent the mean ± SEM (n = 4 mice per group). No significant difference was found. Scale bar, 40 μm. (B) Fluorescence intensity for TWIST, SNAI2 and β-CATENIN immunostaining was quantified using Metamorph™ v7.7.10.0, on the border or the centers of tumors. Data represent the mean ± SEM for n > 3 tumors per genotype. Representative images of SNAI2 staining are shown. Scale bar, 200 μm.

Figure 5: *Bim* deficiency increases the number of metastases. (A) The number of metastases per lung section in PyMT; Bim$^{-/-}$ compared with PyMT; Bim$^{+/-}$ and PyMT; Bim$^{+/+}$ mice (PyMT; Bim$^{+/+}$, n = 12; PyMT; Bim$^{+/-}$, n = 8; and PyMT; Bim$^{-/-}$, n = 18). Data represent mean ± SEM. Similar results were obtained for F2 second generation mice. (B) H&E sections of lungs from PyMT and PyMT; Bim$^{-/-}$mice. Arrows indicate the metastases. Scale bar, 80 μM. (C) Primary tumor weights of PyMT; Bim$^{+/+}$ (n = 25), PyMT; Bim$^{+/-}$ (n = 8) or PyMT; Bim$^{-/-}$ (n = 14) tumors collected at ethical endpoint. The total weight of the different tumors per mouse is represented, since multifocal tumors arise in the PyMT model. Error bars represent mean ± SEM.

Figure 6: Increased survival of *Bim*-deficient cells in the lung microenvironment. (A) Weights and images of the lungs of Rag1$^{-/-}$J mice, one month after i.v. injection of 500,000 cells from PyMT; Bim$^{+/+}$ or PyMT; Bim$^{-/-}$ mice of F2 generation. Data represent the mean ± SEM of n = 12 mice per group, for 3 independent experiments. (B) 500,000 tumor cells from PyMT; Bim$^{+/+}$ or PyMT; Bim$^{-/-}$ were injected in the lungs of Rag1$^{-/-}$J by intratracheal injection. For each experiment, all the mice were sacrificed when the first mouse developed signs of respiratory distress. Left panel: Lungs were harvested and weighed (n > 17 mice per group, 4 independent experiments). Data represents the mean ± SEM. Right panel: H&E sections of the lungs. Scale bar, 40 μm.

Supplementary Figure Legends

Supplementary Figure 1: Effect of *Bim* loss on the host immune system. (A) Analysis of leukocyte number in blood from mice of different genotypes and different genetic backgrounds, as shown. Analysis was performed with the Advia 2120. ND, not determined. Data represent the mean ± SEM for n > 3 mice per group. (B) $Gr1^{+}Mac1^{+}$ myeloid cells per tumor from mice of the indicated genotypes. Error bars represent the mean ± SEM for n = 3 independent experiments. (C) Survival of $Rag1^{-/-}J$ mice after mammary fat pad transplantation with 500,000 tumor cells from PyMT; $Bim^{+/+}$ or PyMT; $Bim^{-/-}$ mice (F2 generation). PyMT; $Bim^{+/+}$, n = 20; PyMT; $Bim^{-/-}$, n = 22. (D) Percentage of $CD31^{+}$ endothelial cells per tumor from mice of the indicated genotypes. Bars represent mean ± SEM for n = 3 independent experiments.

Supplementary Figure 2: Expression of SNAI2 in mouse mammary tumor models. (A) Immunostaining for BIM, SNAI2, TWIST and KI67 at the borders of different mouse tumor models: MMTV-Neu, BALB/c-$p53^{+/-}$ and MMTV-Wnt1. Scale bar, 40 μm. (B) Western blot analysis of SNAI2 expression in pre-neoplastic mammary tissue and tumors for the PyMT, MMTV-Wnt1, MMTV-Neu and BALB/c-$p53^{+/-}$ mouse models. TUBULIN provided a protein loading control. Each sample represents a single tumor. (C) TUNEL assay and immunostaining for cleaved caspase-3 or (D) DAPI, CD31 or KI67 of PyMT; $BIM^{+/+}$ tumor sections. Scale bar, 200 μm.

Supplementary Figure 3: SNAI2 binds to the human BIM promoter. (A) Immunostaining of sections from an adult mammary gland, PyMT tumor and PyMT lung metastasis for SNAI2 and BIM expression. Scale bar, 2 μm. (B) Western blot analysis of SNAI2 and BIM expression in MDA-MB-231 cells expressing either LMS-shLUC or LMS-shSNAI2 knockdown constructs. ACTIN provided a protein loading control. (C) ChIP of SNAI2 on the *BIM* promoter in MDA-MB-231 cells. Antibodies against IgG and anti-SNAI2 were used to immunoprecipitate protein bound to the *BIM* promoter (n = 2 independent experiments). Regions of SNAI2 binding are depicted above. (D)

Representative images of TWIST and β-CATENIN border staining from data analysis in Figure 4B. Scale bar, 200 μm. Inset width: 3 μm.

Supplementary Figure 4: Expression of SNAI2 and BIM in patient xenograft models. (A) Immunostaining for KI67, SNAI2 and BIM at the borders of human tumors: Metaplastic models: 162T and 371T; Triple negative: 110T; ER-positive: 23T. Scale bar, 2 μm. (B) CD31 staining and DAPI assay on sections from 371T and 23T breast cancer xenografts. Scale bar, 200 μm.

Supplementary Figure 5: Increased survival of *Bim*-deficient PyMT tumor cells in the lungs after tail vein injection. Histological sections of $Rag1^{-/-}$J mice 2 hrs, 3 wks or 4 wks after i.v. injection of 500,000 tumor cells from PyMT; $Bim^{+/+}$, PyMT; $Bim^{-/-}$ mice (FVB/N). Scale bar, 40 μm.

Supplementary Figure 6: Loss of BIM increases lung colonization by MDA-MB-231 breast cancer cells. (A) Western blot analysis MDA-MB-231 cells transfected with the control LMS-Ctl or LMS-shBIM (BIM shRNA) knockdown construct. ACTIN was used as a loading control. (B) Mice were injected i.v. with MDA-MB-231 LMS-Ctl or LMS-shBIM cells, then imaged 2, 24 or 48 hrs post-injection ($n = 3$ for no injection, $n = 4$ for LMS-Ctl and LMS-shBIM groups). Error bars represent the SEM. The right panel shows representative IVIS images taken at the indicated time points.

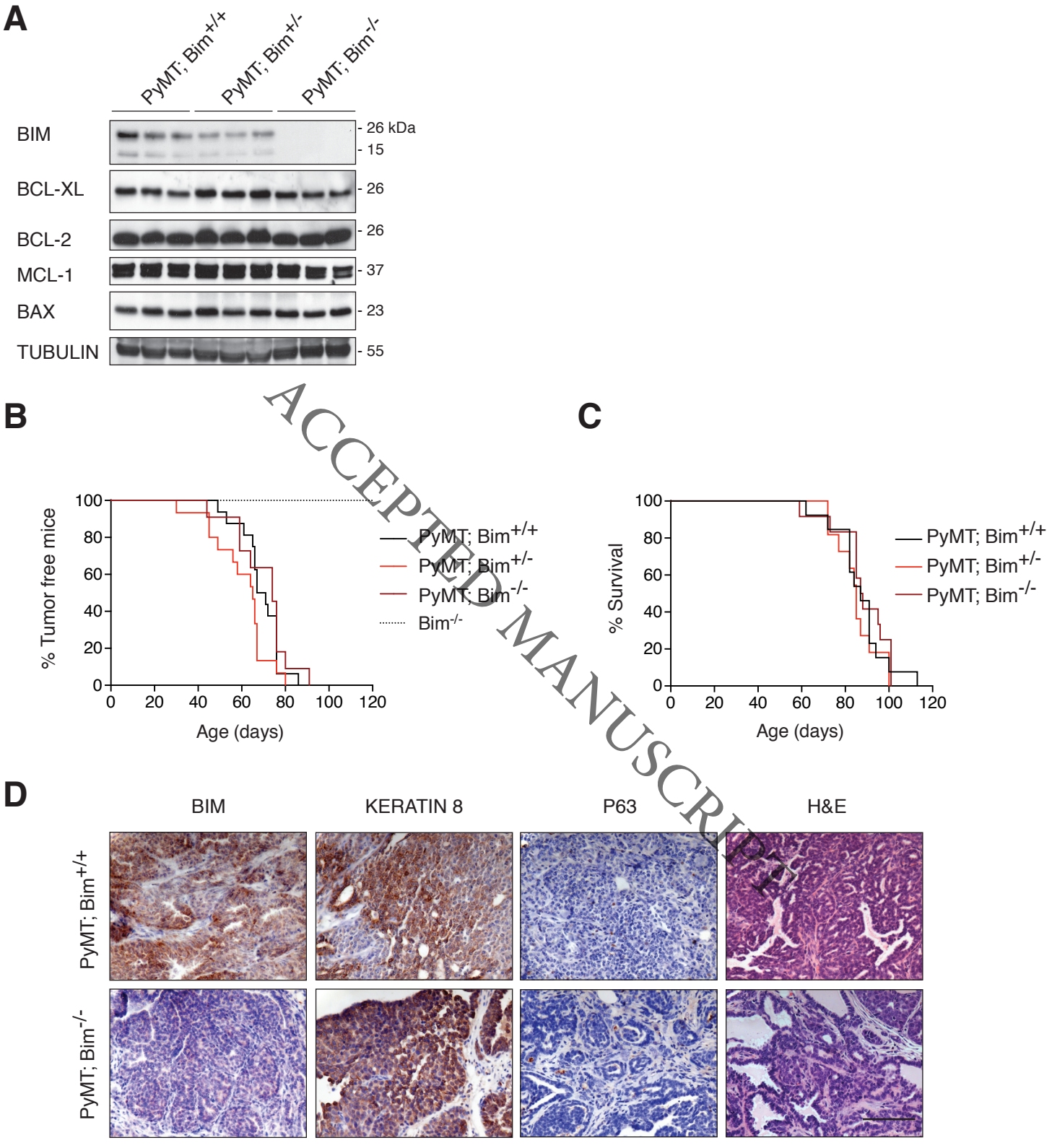

Figure 1

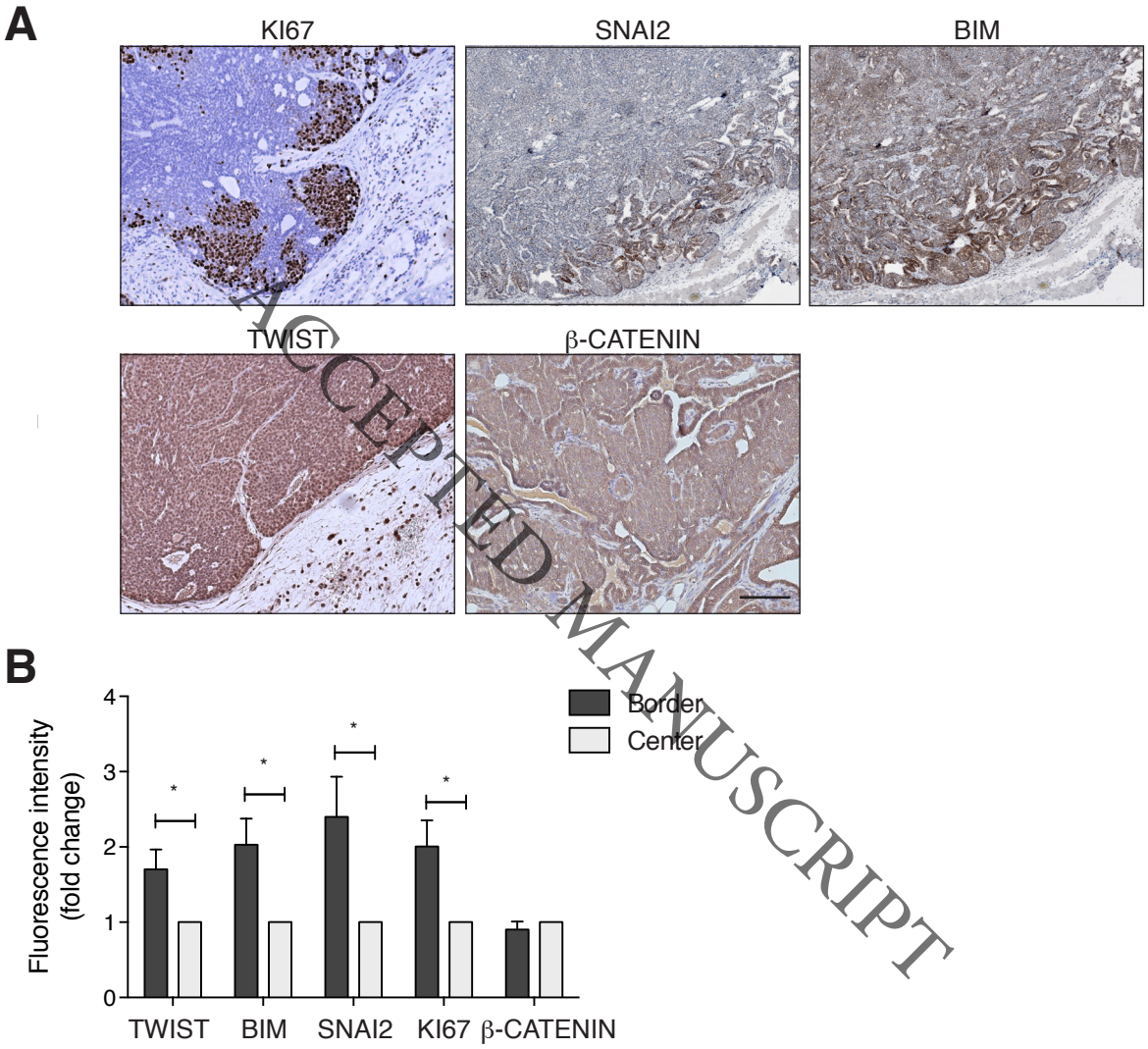

Figure 2

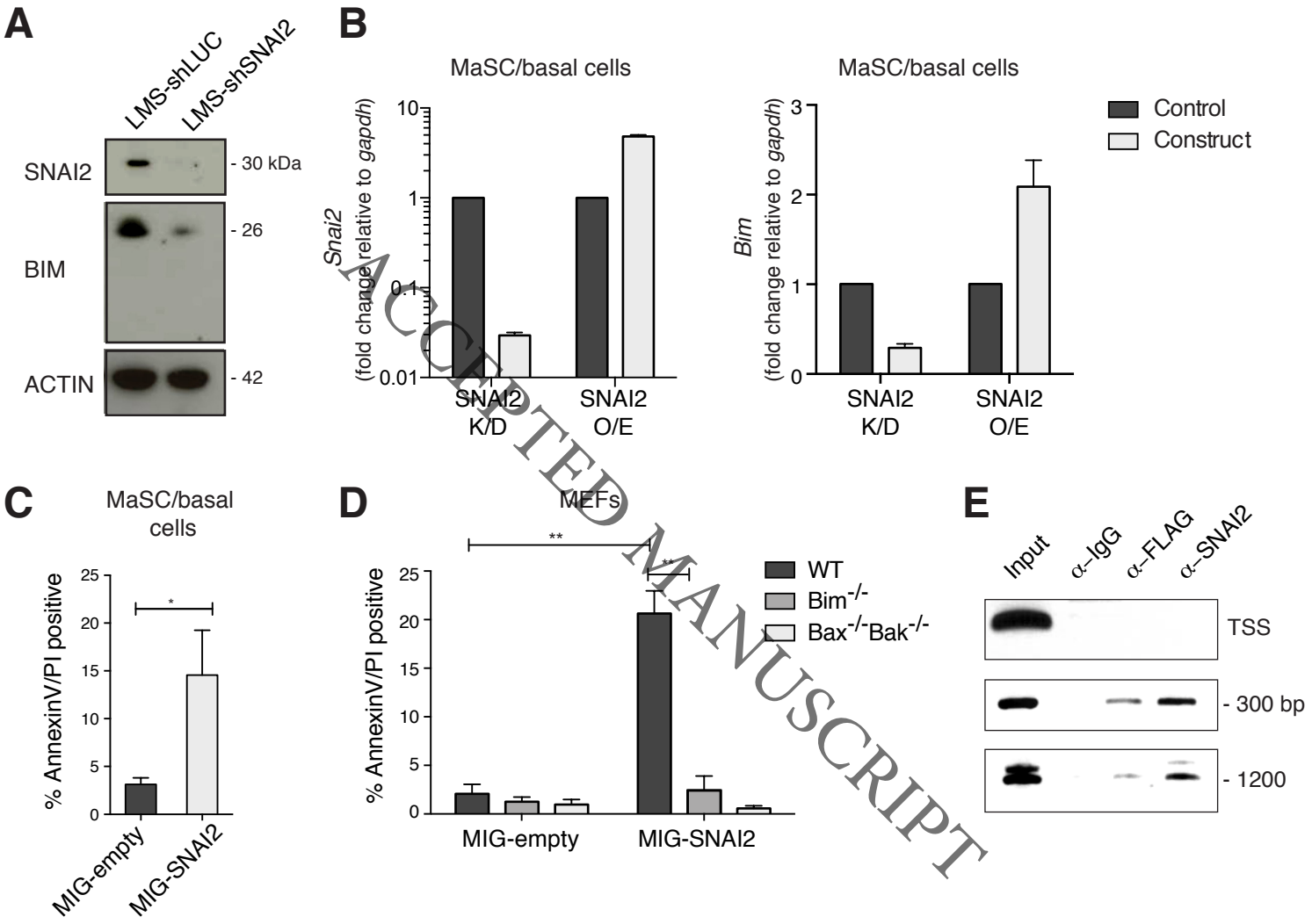

Figure 3

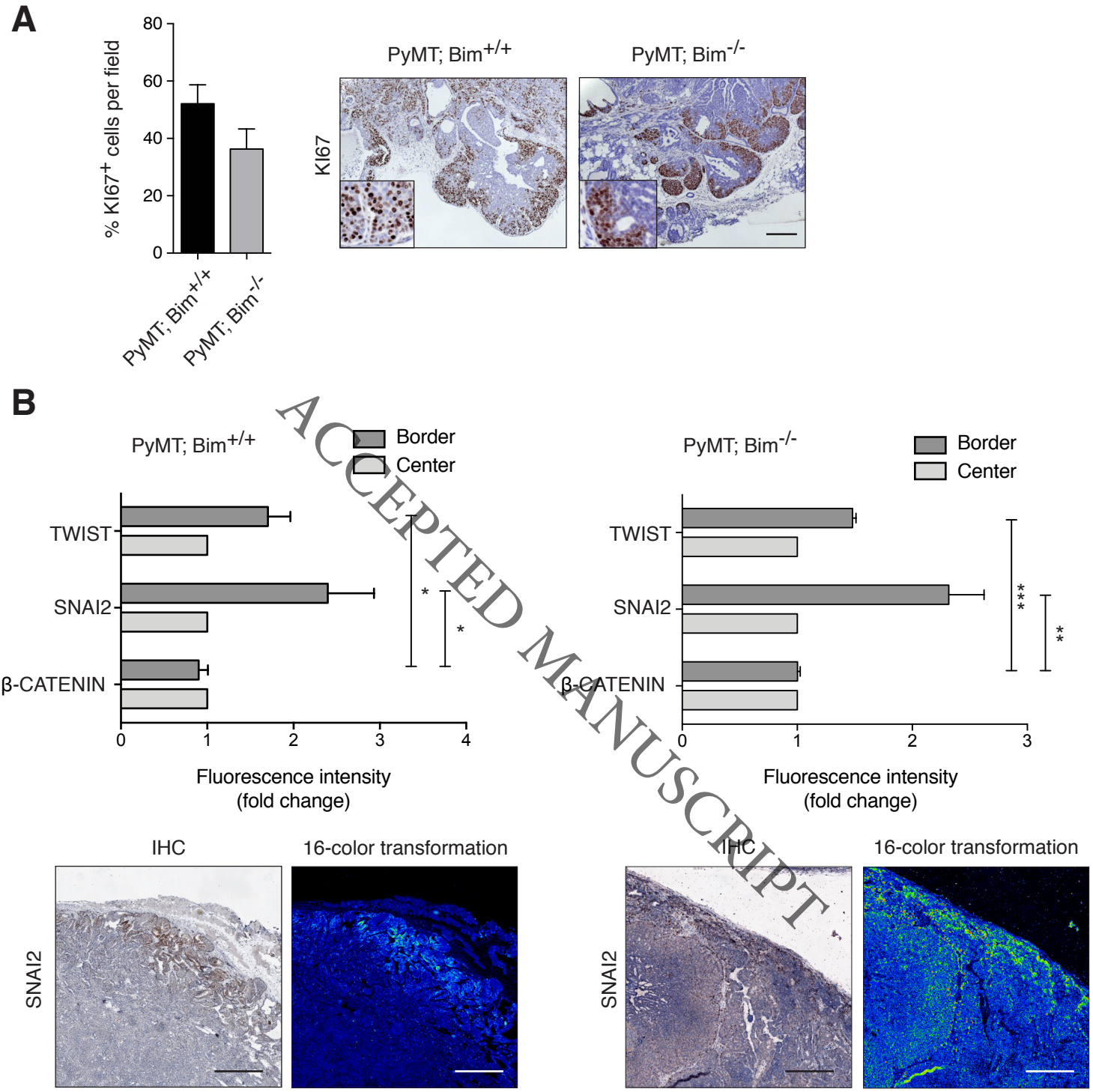

Figure 4

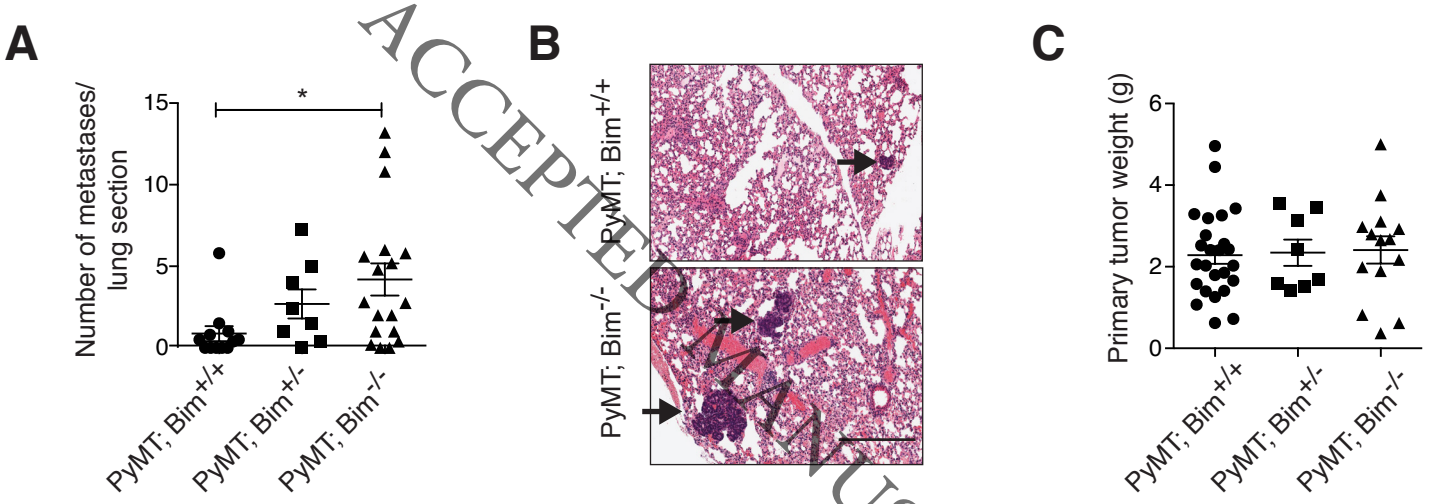

Figure 5

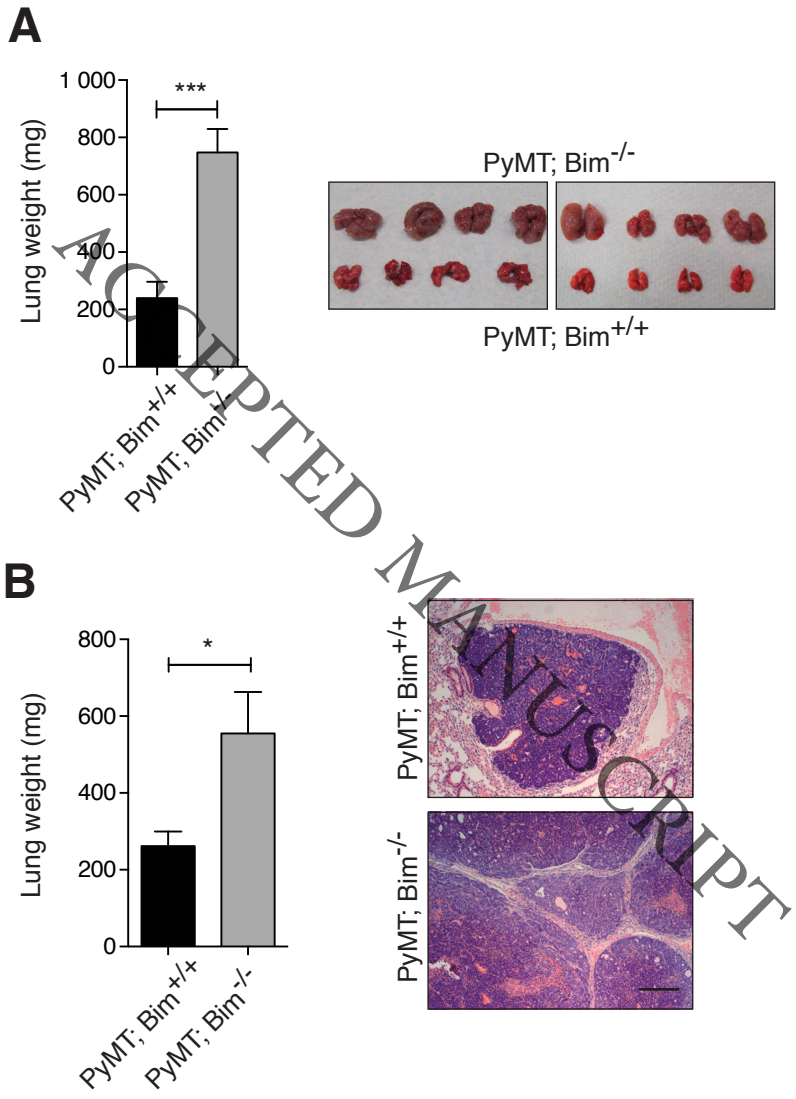

Figure 6

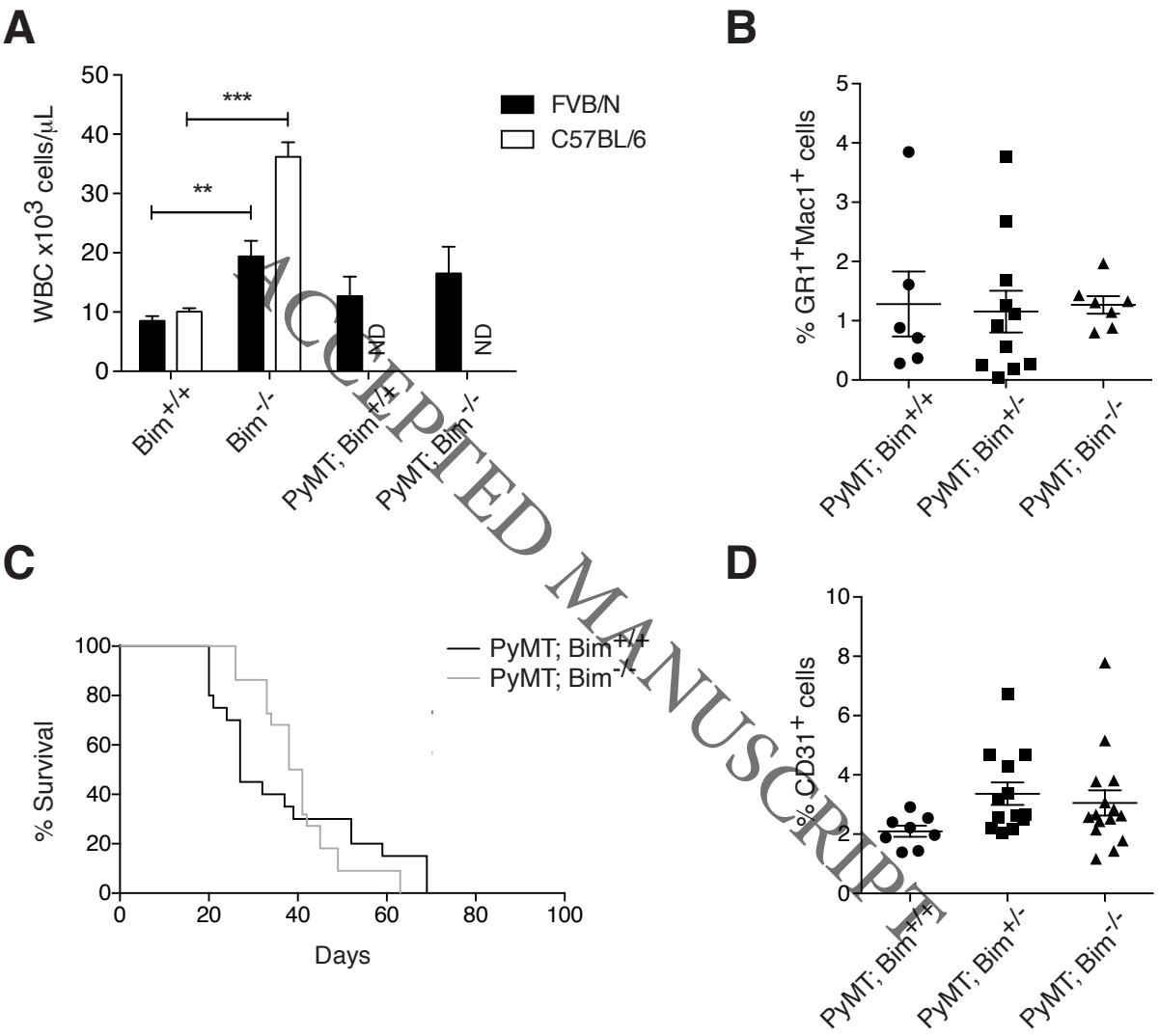

Supplementary Figure 1

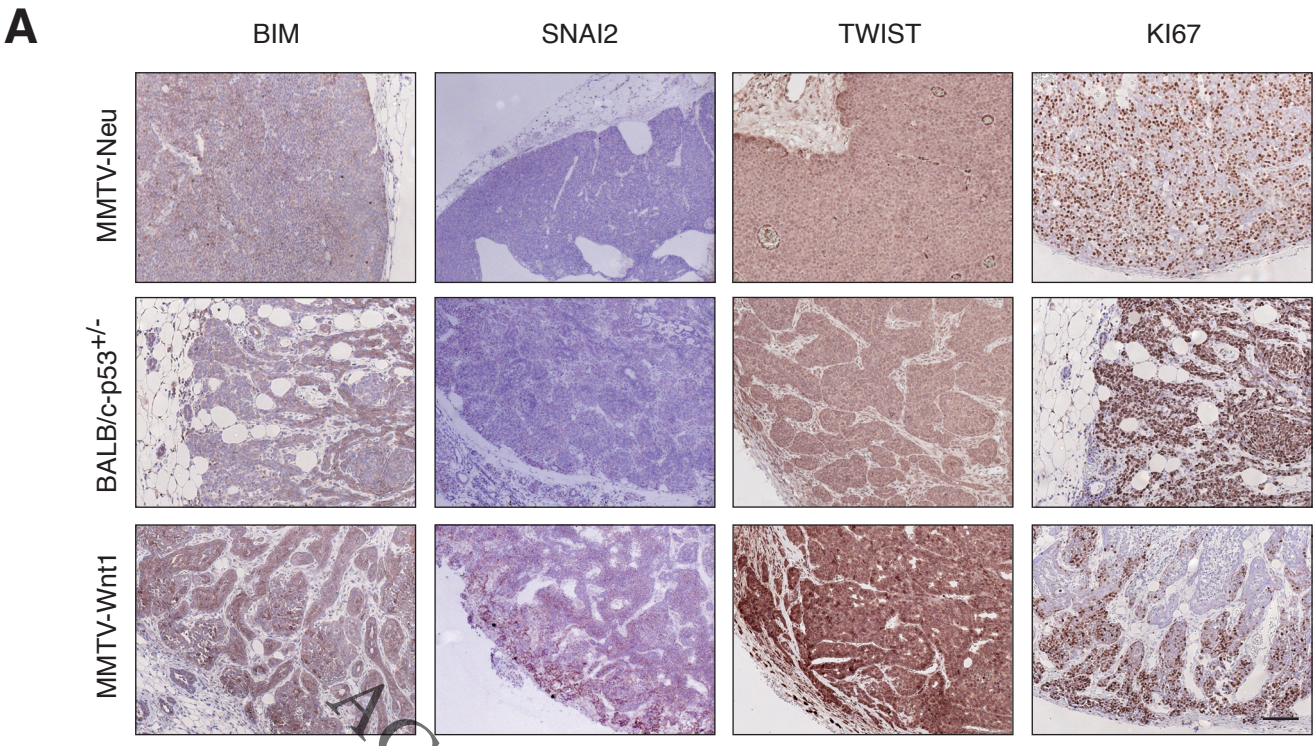

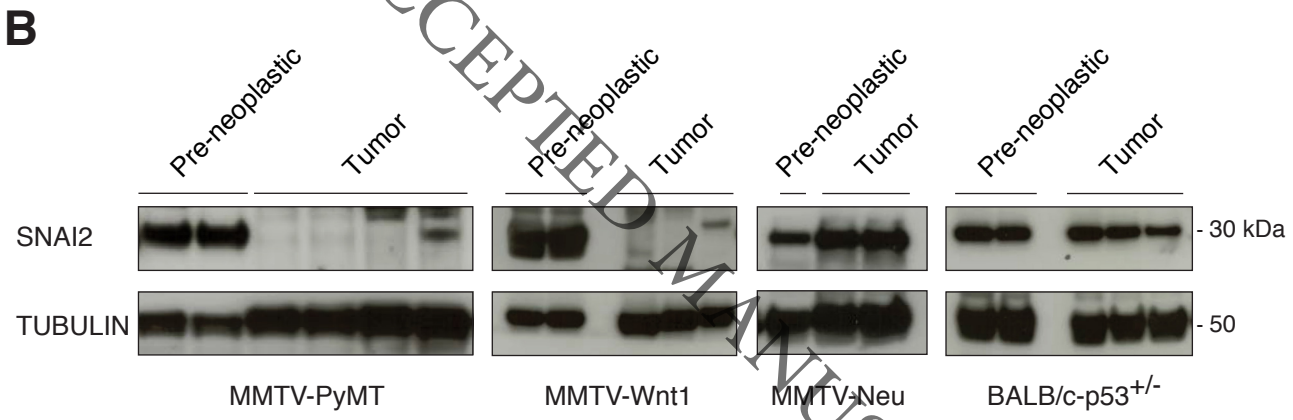

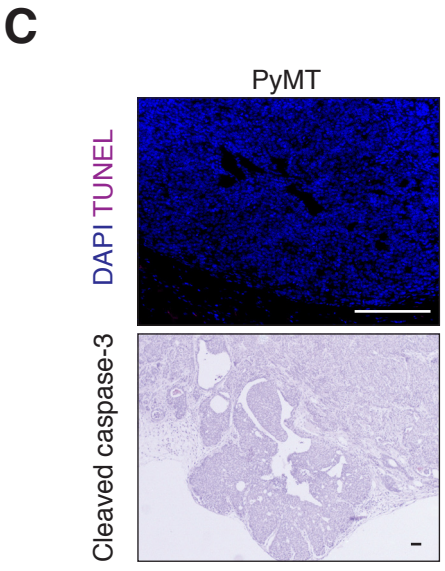

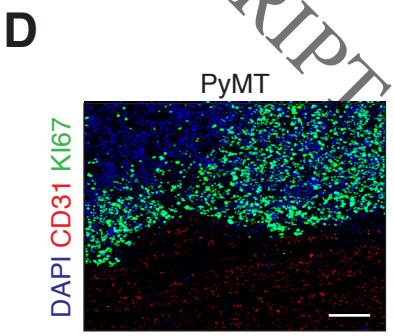

Supplementary Figure 2

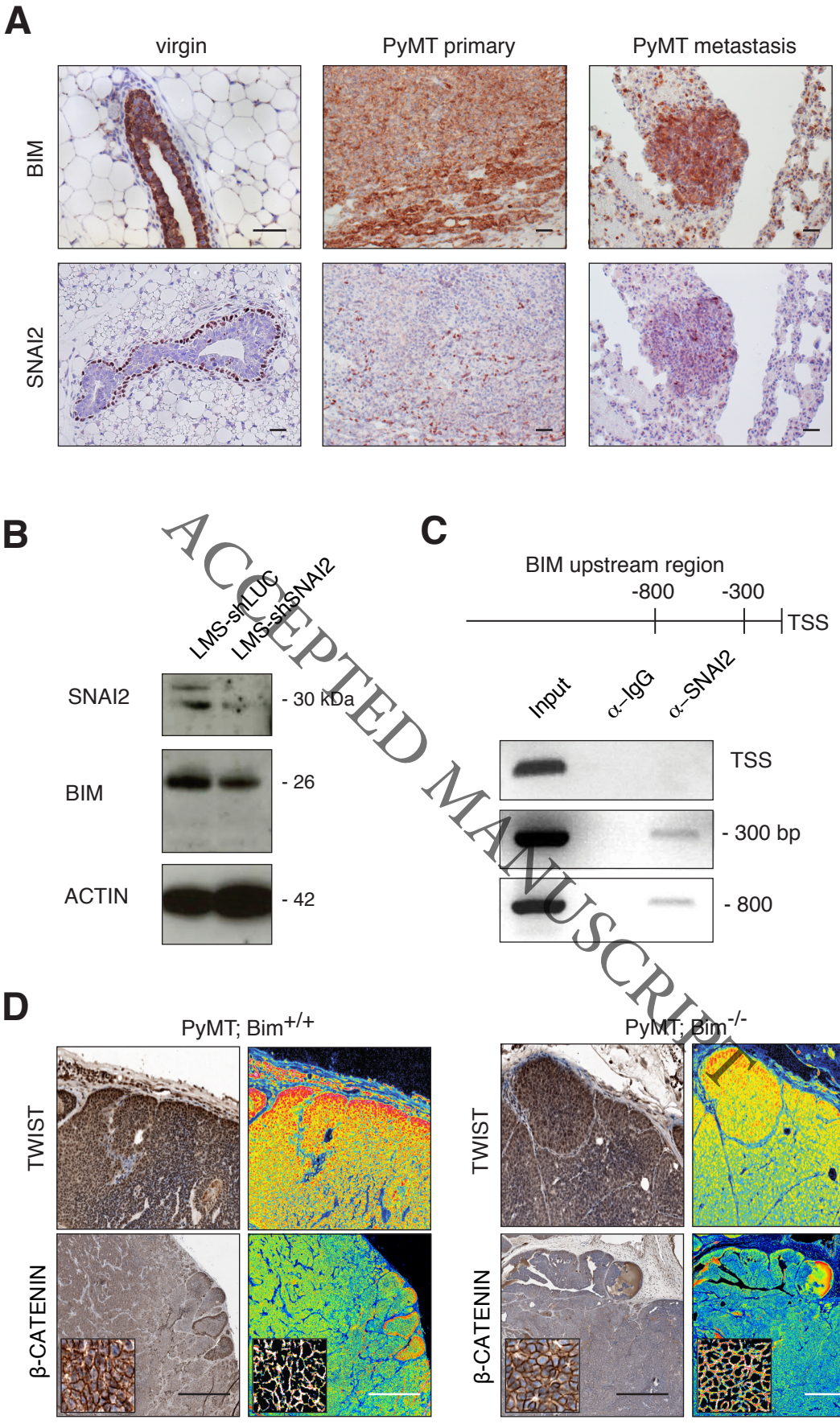

Supplementary Figure 3

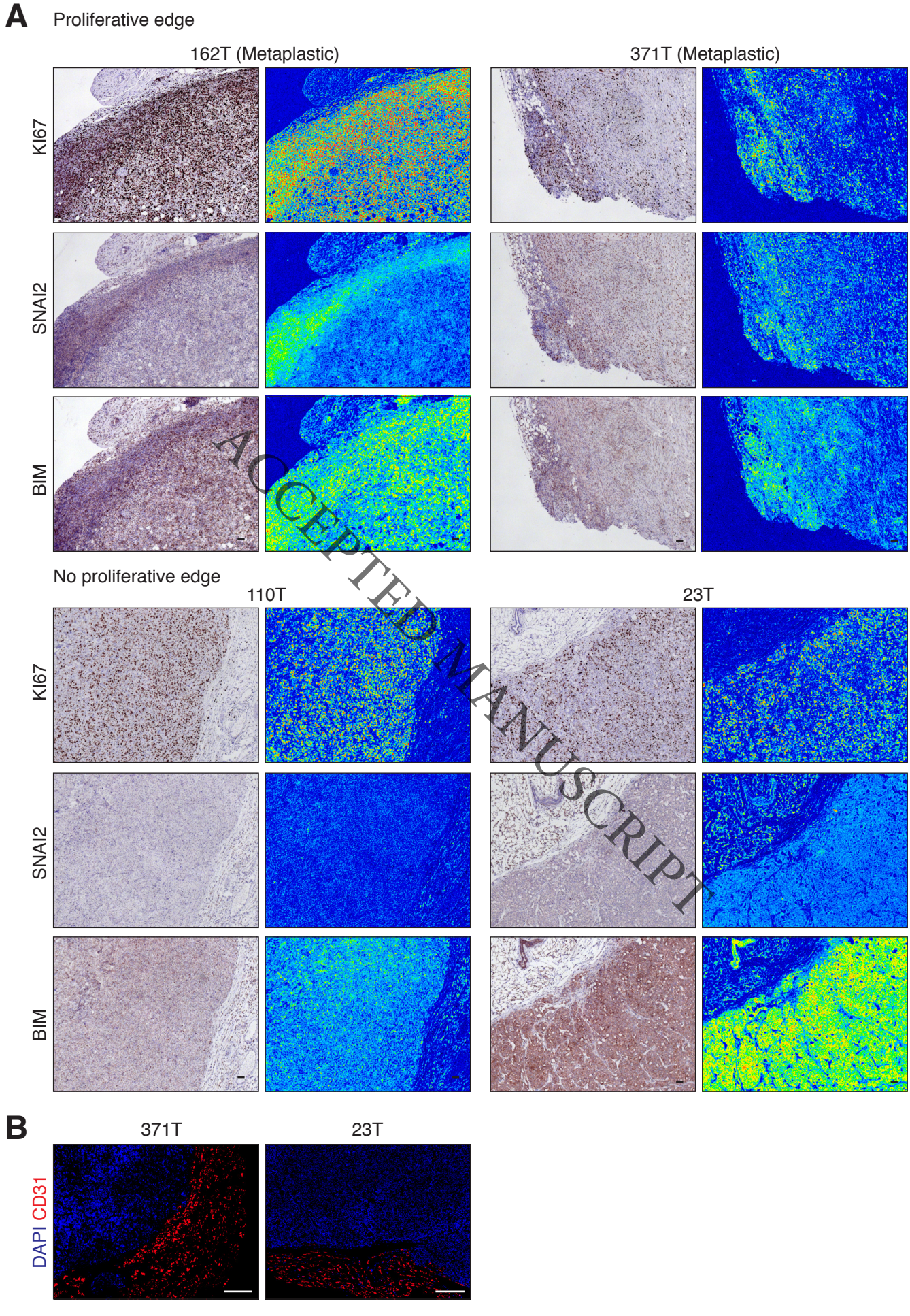

Supplementary Figure 4

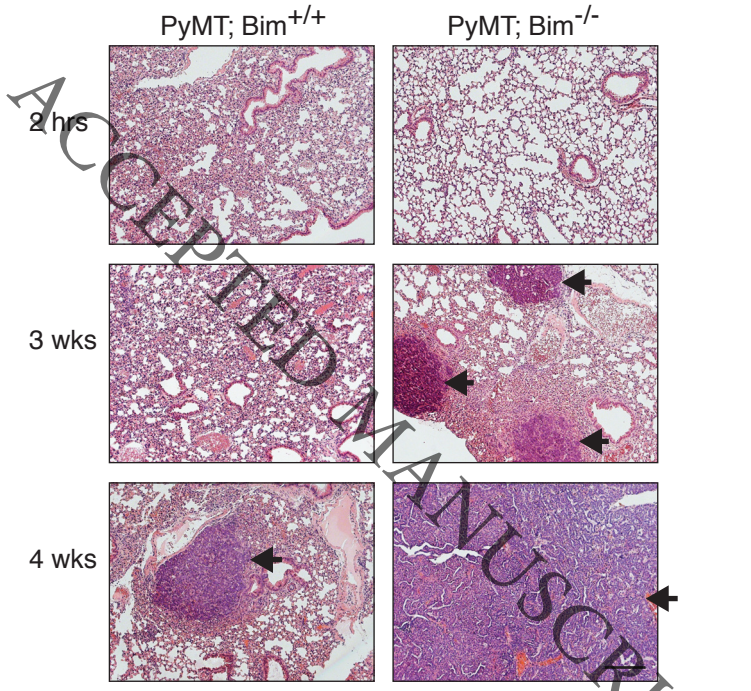

Supplementary Figure 5

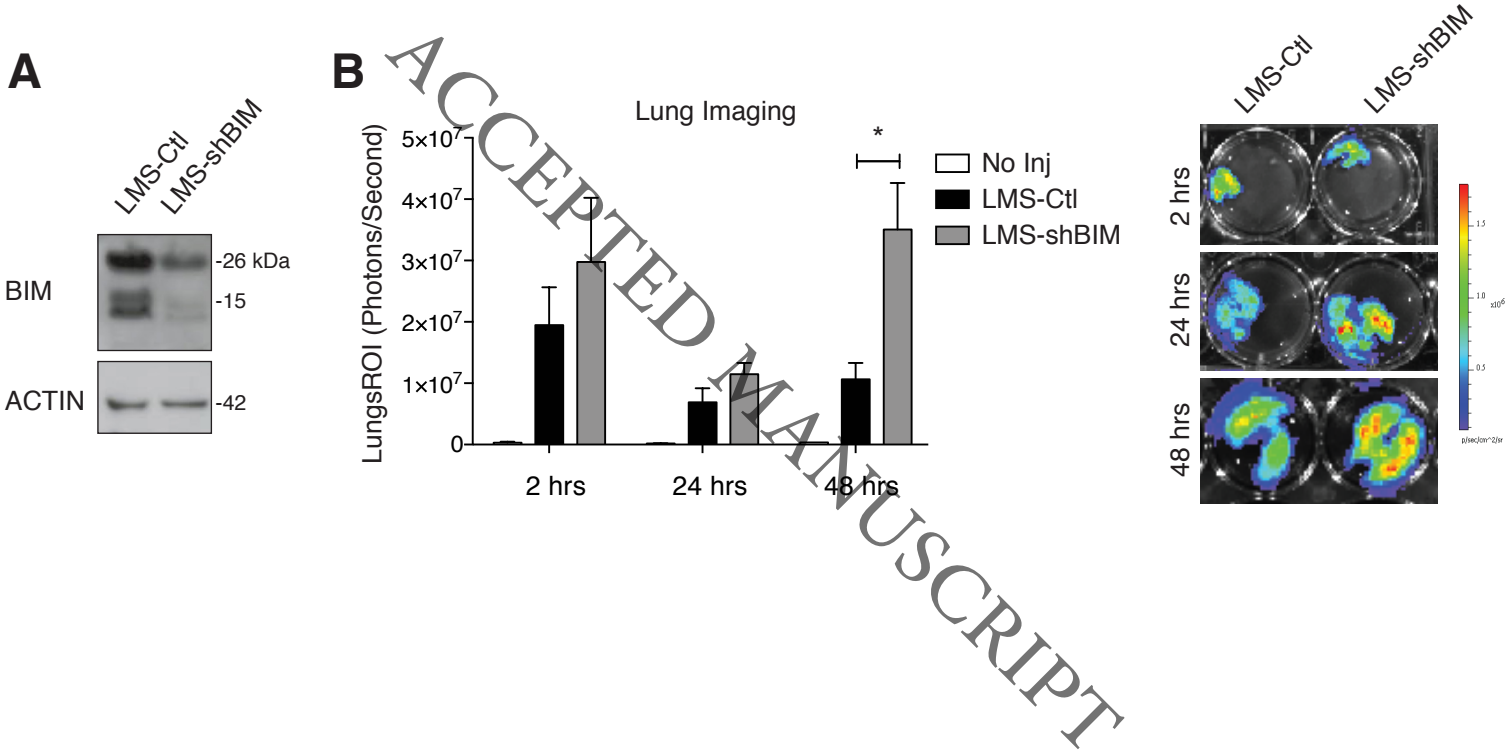

Supplementary Figure 6